Mapping of treatment-induced apoptosis in normal structures: ^{99m}Tc-Hynic-rh-annexin V SPECT and CT image fusion

Marina S. Kartachova[1], Renato A. Valdés Olmos[1], Rick L. M. Haas[2], Frank J. P. Hoebers[2], Michiel W. van den Brekel[3], Nico van Zandwijk[4], Marcel van Herk[2], Marcel Verheij[2]

[1] Department of Nuclear Medicine, The Netherlands Cancer Institute/Antoni van Leeuwenhoek Hospital, Plesmanlaan 121, 1066 CX Amsterdam, The Netherlands
[2] Department of Radiotherapy, The Netherlands Cancer Institute/Antoni van Leeuwenhoek Hospital, Amsterdam, The Netherlands
[3] Department of Head and Neck Oncology and Surgery, The Netherlands Cancer Institute/Antoni van Leeuwenhoek Hospital, Amsterdam, The Netherlands
[4] Department of Thoracic Oncology, The Netherlands Cancer Institute/Antoni van Leeuwenhoek Hospital, Amsterdam, The Netherlands

Received: 29 September 2005 / Accepted: 20 December 2005 / Published online: 4 April 2006

Abstract. *Purpose:* The purpose of this study was to map treatment-induced ^{99m}Tc-Hynic-rh-annexin V uptake in normal tissues using co-registration of SPECT and CT.
Methods: Nineteen patients (11 male, 8 female, mean age 57 years) with various malignant tumours (12 lymphomas, four non-small cell lung cancers and three head and neck squamous cell carcinomas) underwent ^{99m}Tc-Hynic-rh-annexin V scintigraphy and CT before and within 48 h after the start of anticancer therapy. SPECT and CT were performed separately, with the patient in a reproducible position. Volume-based automated and manual methods were used to match functional and anatomical data. SPECT/CT co-registration was used to evaluate treatment-induced changes in the normal structures.
Results: A significant radiation field-related increase in early post-treatment ^{99m}Tc-Hynic-rh-annexin V uptake in salivary glands and bone marrow was detected in eight of nine patients. Radiation field-related increase in bone marrow activity above the baseline value was detected in all 13 irradiated patients. A minimal, symmetrical increase in activity in the salivary glands was detected after the initial course of platinum-based chemotherapy, and a diffuse prominent increase in ^{99m}Tc-Hynic-rh-annexin V in the bone marrow was detected in all cases. Precise delineation between the tumour and normal tissue tracer accumulation was accomplished in all cases using SPECT/CT co-registered volumes, enhanced by the "colourwash" technique.
Conclusion: Mapping of early treatment-related changes in annexin V uptake by SPECT/CT co-registration permits accurate evaluation of tracer distribution in normal structures and precise delineation from tumour uptake. The associations between tracer distribution in the normal tissues and treatment regimen found in this study may contribute to the evaluation of dose–effect relations in various treatment schedules.

Keywords: Apoptosis – Annexin V – Matching – SPECT/CT

Eur J Nucl Med Mol Imaging (2006) 33:893–899
DOI 10.1007/s00259-006-0070-1

Renato A. Valdés Olmos (✉)
Department of Nuclear Medicine,
The Netherlands Cancer Institute/Antoni van Leeuwenhoek Hospital,
Plesmanlaan 121,
1066 CX Amsterdam, The Netherlands
e-mail: r.valdes@nki.nl
Tel.: +31-20-5122289, Fax: +31-20-5122225

Introduction

Advanced stage cancer remains an important challenge in oncology. For the majority of patients with locally advanced and metastatic disease, chemotherapy and/or radiotherapy is the standard treatment option. However, these anticancer regimens are frequently associated with side-effects while recurrence rates remain high. Thus, it is very important to identify those patients who will benefit from the treatment and those who will not. It is widely accepted that apoptosis contributes to tumour response to anticancer therapy and that defects in the apoptotic pathways play a key role in tumour resistance to radiotherapy and most, if not all, chemotherapeutic drugs. ^{99m}Tc-Hynic-rh-annexin V scintigraphy (TAS) allows in vivo monitoring of apoptosis [1–3] and early changes in the annexin V tumour uptake correlate significantly with outcome [4–6]. In our previous studies we showed that

TAS might be useful early during the course of treatment as a predictive test for treatment response [5]. Despite these promising results, evaluation of TAS data is complicated by a low tumour-to-background ratio and the spatial resolution of the gamma camera. Registration of functional single-photon emission computed tomography (SPECT) and anatomical computed tomography (CT) information is widely recognised as a clinically relevant method to improve the anatomical definition of SPECT [7–9].

In this study we evaluated ^{99m}Tc-Hynic-rh-annexin V distribution in normal tissues before and early after the start of anticancer therapy. SPECT/CT fusion was applied to improve the anatomical resolution of SPECT and to ensure accurate delineation between the tumour and areas of physiological tracer accumulation.

Materials and methods

Patients

The study population comprised 19 consecutive patients (11 male, 8 female, mean age 57 years) with various malignant tumours—12 lymphomas, four non-small cell lung cancer (NSCLCs) and three head and neck squamous cell carcinomas (H&NSCC)—who were enrolled in two separate studies (multicentre and physician-sponsored) with the final aim of evaluating the predictive value of TAS in haematological and solid tumours. Patient characteristics are summarised in Table 1. All patients were older than 18 years, and all had a histologically or cytologically confirmed extra-abdominal malignant tumour, one or more measurable lesions with at least one lesion larger than 2 cm, a World Health Organisation performance score of 1 or 2 and a life expectancy of more than 16 weeks. The study was approved by the institutional ethical committee. All patients received extensive information about the purpose of the study and gave their signed informed consent before enrolment.

^{99m}Tc-Hynic-rh-annexin V scintigraphy

TAS was performed within 2 weeks before treatment and was repeated within 48 h after the start of treatment. Patients received an average of 855 MBq (range 676–1,117 MBq) of ^{99m}Tc-Hynic-rh-annexin V (Theseus Imaging Corporation, Boston, MA, USA) intravenously 4 h prior to the planar and SPECT imaging. SPECT images were acquired according to the standard protocol: step and shoot mode, one step per 3°, 30 s per frame, matrix size 128×128) using a dual-head gamma camera (Genesis, Philips, Best, The Netherlands) equipped with low-energy, high-resolution collimators. Raw SPECT data were reconstructed using an iterative algorithm and postfiltered using a Butterworth filter (cut-off frequency 0.35, order 5).

Computed tomography

Spiral CT (Tomoscan AVE1, Philips, Best, The Netherlands or HiSpeed CT, GE Medical Systems, USA) was performed in all cases within 4 weeks before the start of treatment in order to determine the tumour localisation and its local extension.

Matching

SPECT and CT were performed separately, with the patient in a reproducible position using an immobilisation mask or a fixed supine position. Reconstructed data were transferred to an in-house developed PC-based image registration workstation (Conquest Workstation) in DICOM format. SPECT/SPECT and SPECT/CT co-registration was performed using a volume match. The interactive mode of the fusion software was used, allowing the user to both automatically and manually rotate the SPECT scan and produce the best visual overlay of the two sets of images. The CT and SPECT images were then displayed side by side. Matching accuracy was verified based on the alignment of the bony structures and liver, present on both scans. The "colourwash" technique was used on observer demand to superimpose colour-coded SPECT data onto a two-dimensional slice through the anatomical volume, in which the colour at any given point of the composite image was determined by the pixel count value on the SPECT image at that point. Image level and window of SPECT image were adjusted to represent the injected dose and normalised.

Reading procedure

SPECT/SPECT and SPECT/CT co-registrations were visually examined to evaluate treatment-induced changes in the non-tumour structures after appropriate correction for injected dose. A consensus reading of the co-registered data sets was made by two nuclear medicine physicians, unaware of patient identity and treatment outcome, using the standard procedure described in our previous publication [5]. Real-time analysis of co-registered baseline and follow-up SPECT volumes and SPECT/CT images, enhanced by the colourwash technique, was applied for precise delineation between the tumour and areas of prominent physiological uptake, including bone structures and salivary glands.

Physiological areas of tracer accumulation were correlated with the anatomical structures (salivary glands, bone marrow) and uptake was classified as decreased, stable or increased, compared with baseline values. Agreement between the observers regarding normal tissue uptake was achieved in all cases. In the event of disagreement regarding the grade of tumour uptake (two cases), the images were jointly reviewed and agreement was reached by consensus.

Results

Physiological biodistribution

Physiological biodistribution of ^{99m}Tc-Hynic-rh-annexin V, consisting of prominent accumulation in the salivary glands, bone marrow, liver, spleen, kidneys and bladder [10, 11], was detected in all cases. Visual analysis of the post-treatment scans demonstrated no significant changes in the visceral tracer uptake. Changes in salivary gland and bone marrow uptake were strongly dependent on the treatment modality.

Table 1. Patient characteristics

No.	Gender	Age (yrs)	Location	Histology	ΔU tumour[a]	Bone marrow uptake	Salivary gland uptake	Treatment modality	Response
1	m	64	Right upper lobe, mediastinum	NSCLC	Stable	Diffuse increase	Slight symmetrical increase	Pt-based chemotherapy	SD
2	m	58	Right upper lobe, mediastinum	NSCLC	Stable	Diffuse increase	Slight symmetrical increase	Pt-based chemotherapy	SD
3	f	56	Left upper lobe	NSCLC	Increased	Diffuse increase	Slight symmetrical increase	Pt-based chemotherapy	PR
4	m	51	Right upper lobe	NSCLC	Decreased	Diffuse increase	Slight symmetrical increase	Pt-based chemotherapy	PD
5	m	26	Tongue base, cervical lymph nodes, left	H&NSCC	Increased	Field-related increase	Intense symmetrical field-related increase	Concurrent chemoradiation	CR
6	m	54	Tongue base, cervical lymph nodes, both sides	H&NSCC	Increased	Field-related increase	Intense symmetrical field-related increase	Concurrent chemoradiation	CR
7	m	55	Right tonsil, cervical lymph nodes, level V, both sides	H&NSCC	Increased	Field-related increase	Intense symmetrical field-related increase	Radiotherapy	CR
8	f	42	Left tonsil, cervical lymph nodes, level III/IV	fNHL	Increased	Field-related increase	Intense symmetrical field-related increase	Radiotherapy	CR
9	f	60	Cervical lymph nodes, level III/IV, left	fNHL	Increased	Field-related increase	Intense symmetrical field-related increase	Radiotherapy	CR
10	m	47	Inguinal lymph nodes, left	fNHL	Stable	Field-related increase		Radiotherapy	PD
11	f	43	Supra-auricular lymph nodes, right	fNHL	Increased	Field-related increase	No uptake (RT 1 year ago)	Radiotherapy	CR
12	m	79	Cervical lymph nodes, level V	fNHL	Increased	Field-related increase	Intense symmetrical field-related increase	Radiotherapy	CR
13	m	83	Axillary lymph nodes, left	fNHL	Increased	Field-related increase		Radiotherapy	PR
14	f	65	Cervical lymph nodes, level III/IV	fNHL	Increased	Field-related increase	Intense symmetrical field-related increase	Radiotherapy	CR
15	f	42	Axillary lymph nodes, left	fNHL	Increased	Field-related increase		Radiotherapy	PR
16	f	60	Cervical lymph nodes, level III/IV/V	fNHL	Increased	Field-related increase	Intense symmetrical field-related increase	Radiotherapy	PR
17	m	74	Cervical lymph nodes, all levels, both sides	fNHL	Increased	Field-related increase	Intense symmetrical field-related increase	Radiotherapy	CR
18	f	57	Inguinal lymph nodes, right	fNHL	Increased	Field-related increase		Radiotherapy	PR

Table 1. (continued)

No.	Gender	Age (yrs)	Location	Histology	ΔU tumour[a]	Bone marrow uptake	Salivary gland uptake	Treatment modality	Response
19	m	61	Axillary lymph nodes, right	fNHL	Increased	Field-related increase		Radiotherapy	PR

m male, *f* female, *fNHL* follicular non-Hodgkin's lymphoma, *NSCLC* non-small cell lung cancer, *H&NSCC* head and neck squamous cell carcinoma, *RT* radiotherapy, *Pt* platinum, *CR* complete response, *PR* partial response, *SD* stable disease, *PD* progressive disease

[a] Change in the annexin V tumour uptake, assessed as the difference between early post-treatment uptake and baseline uptake

Changes related to radiotherapy

Fifteen patients with malignant lymphoma (n=12) or H&NSCC (n=3) received radiotherapy or concurrent chemoradiation. Salivary glands were included in the radiation field in nine of these patients. A significant increase in early post-treatment accumulation of ^{99m}Tc-Hynic-rh-annexin V in salivary glands within the radiation field was detected in eight of nine patients. An example of asymmetrical increase in annexin V uptake in the salivary glands 24 h after the start of parotid gland-sparing radiotherapy is presented in Fig. 1. Figure 2 illustrates short-term and long-term (approximately 1 year after radiotherapy) effects of the parotid gland irradiation. In four patients, the salivary glands were not included in the radiation field. In these cases we detected a minimal increase in parotid activity compared with pretreatment values.

A significant increase in bone marrow activity above the baseline value was detected within the radiation field (Fig. 3c–f) in all 13 patients.

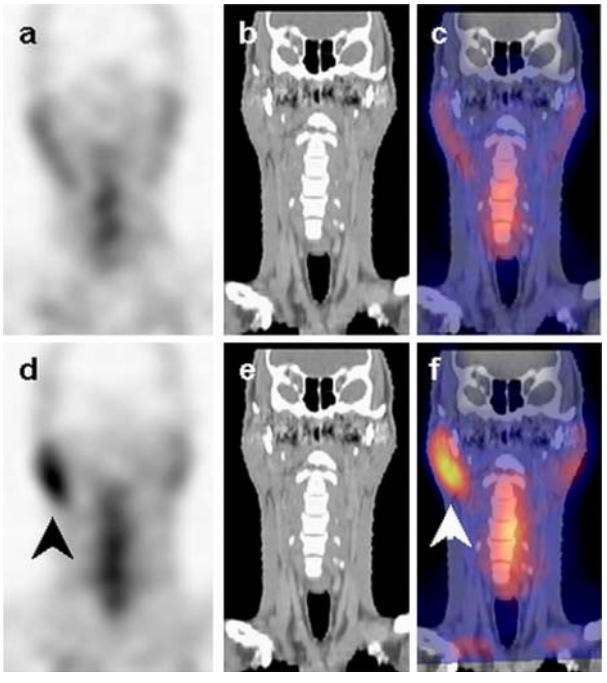

Fig. 1. Changes in salivary gland uptake after "parotid-sparing" radiotherapy (left side spared). **a**–**c** Baseline ^{99m}Tc-Hynic-rh-annexin V scan of a 55-year-old male with a squamous cell carcinoma of the hypopharynx, performed 4 days before the initiation of parotid-sparing chemoradiation, demonstrates symmetrical weak annexin V uptake in both parotid glands. **d**–**f** Follow-up scan performed 48 h after the start of treatment shows intense tracer uptake in the right parotid gland (*arrowheads*), while the uptake on the left (spared) side remains weak

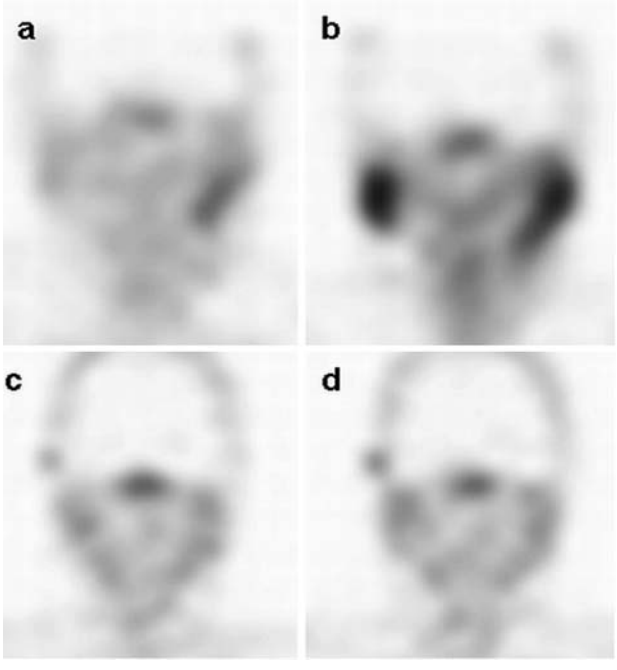

Fig. 2. Radiotherapy-induced changes in the salivary glands. **a**, **b** Follicular NHL in a 43-year-old female with enlarged cervical lymph nodes, at level II–III on the left side, before (**a**) and 48 h after (**b**) the start of low-dose radiotherapy, demonstrating a diffuse symmetrical increase in annexin V accumulation in the salivary glands. **c**, **d** The same patient 1 year later: images obtained before (**c**) and 48 h after (**d**) the start of low-dose radiotherapy due to recurrence of NHL in the right supra-auricular area. Note the increased tumour uptake of ^{99m}Tc-Hynic-rh-annexin V tumour on both scans and the weak stable symmetrical tracer accumulation in the salivary glands

Changes related to chemotherapy

Four patients with NSCLC received platinum-based chemotherapy. A minimal but symmetrical increase in activity in the salivary glands was detected after the initial course of treatment (Fig. 4) and a diffuse prominent increase in ^{99m}Tc-Hynic-rh-annexin V uptake in the bone marrow (Fig. 3a,b) was detected in all cases.

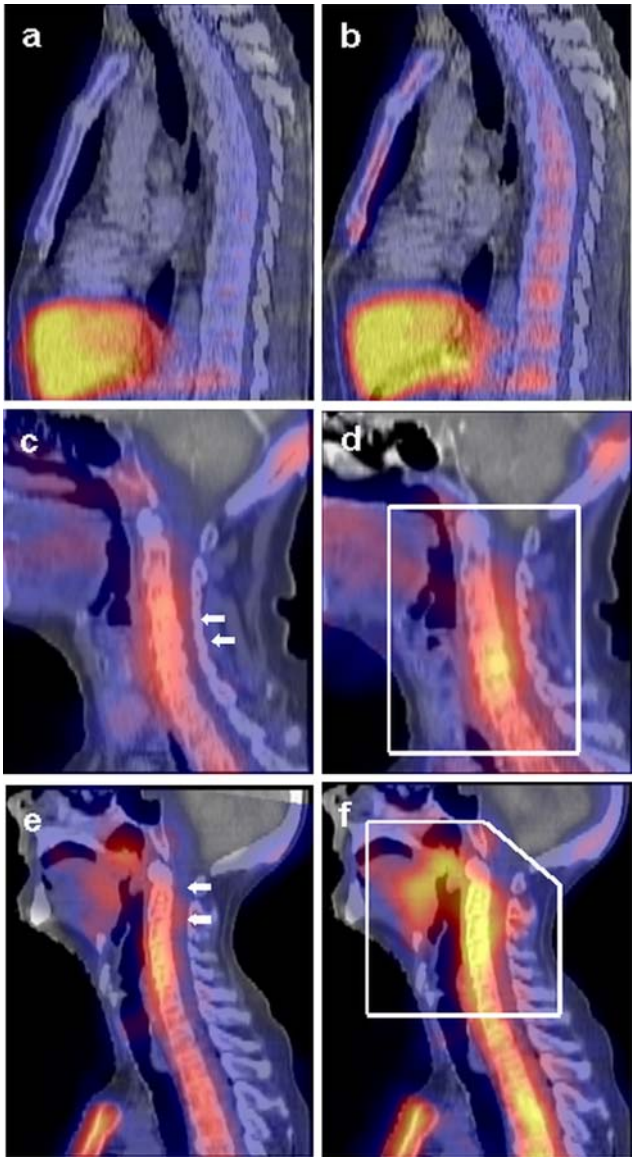

Fig. 3. Changes in the bone marrow uptake after chemotherapy and/or radiotherapy (SPECT/CT fusion). **a** Baseline and **b** follow-up ^{99m}Tc-Hynic-rh-annexin V scans of a 51-year-old male with NSCLC performed 1 week before and 24 h after the initial course of platinum-based chemotherapy, demonstrate a diffuse increase in bone marrow activity. **c** Baseline and **d** follow-up ^{99m}Tc-Hynic-rh-annexin V scans of a 60-year-old female with NHL (cervical lymph nodes at level III/IV, left side) performed 2 weeks before and 48 h after the start of radiotherapy, show a local increase in annexin V accumulation in the cervical spine (*arrows*; white contour corresponds to the radiation field). **e** Baseline and **f** follow-up ^{99m}Tc-Hynic-rh-annexin V scans of a 54-year-old male with H&NSCC performed 1 week before and 48 h after the start of concurrent chemoradiation show a diffuse increase in bone marrow uptake (*arrows*), with maximum uptake in the irradiated area (white contour corresponds to the radiation field)

^{99m}Tc-Hynic-rh-annexin V tumour uptake

Changes in the annexin V tumour uptake (ΔU), assessed as the difference between the early post-treatment uptake ($U_{posttreatment}$) and baseline uptake ($U_{baseline}$), in relation to treatment modality and clinical outcome are summarised in Table 1.

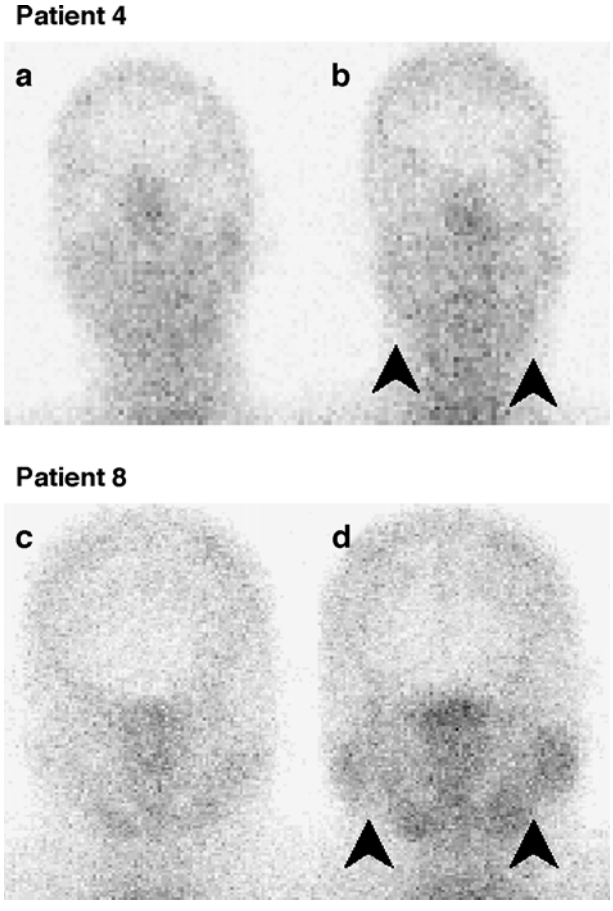

Fig. 4. Chemotherapy- and radiotherapy-induced changes in salivary glands. **a**, **b** Planar images obtained in a 51-year-old male (patient no. 4, Table 1) 4 h after the intravenous injection of ^{99m}Tc-Hynic-rh-annexin V, before (**a**) and 24 h after (**b**) the start of platinum-based chemotherapy. A minimal, symmetrical increase in activity in the salivary glands is observed (*arrows*). **c**, **d** Planar images obtained in a 42-year-old female (patient no. 8, Table 1) 4 h after the intravenous injection of ^{99m}Tc-Hynic-rh-annexin V, before (**c**) and 48 h after (**d**) the start of radiotherapy. A moderate symmetrical increase in activity in the salivary glands is demonstrated (*arrows*)

Discussion

In vivo monitoring of apoptosis in patients with advanced or metastatic cancer is a promising assay to identify those patients who will benefit from the treatment and those who will not. ^{99m}Tc-Hynic-rh-annexin V scintigraphy (TAS) allows in vivo monitoring of apoptosis, and early changes in the annexin V tumour uptake correlate significantly with outcome [4–6].

The group of Haas et al. from the Netherlands Cancer Institute has demonstrated that in patients with low-grade lymphoma, ^{99m}Tc-annexin-V tumour uptake before and early after the start of low-dose radiotherapy was concordant with the appearance of apoptotic morphology as determined by fine-needle aspiration biopsy [12]. In the subsequent publication we focussed on annexin V tumour uptake and demonstrated that TAS might be useful early during the course of treatment as a predictive test for treatment response [5]. Although these results are promising, evaluation of TAS data is complicated by a low tumour-to-background ratio and the spatial resolution of the gamma camera.

In the present work we evaluated a fusion model, applied for visual evaluation of TAS results, and concentrated on the mapping of the therapy-induced changes in annexin V accumulation in the normal tissues to allow better differentiation of tumour and non-tumour uptake. Precise localisation of increased tracer uptake (pathological and physiological) within the anatomical frames is made possible by the additional landmarks depicted on the CT images. Use of the colourwash technique enhances evaluation of the functional SPECT data, seen as a coloured splash on the original CT, and allows exact delineation between the tumour and areas of prominent physiological uptake. This is particularly important for the evaluation of the annexin V uptake in patients with head and neck tumours, who demonstrate prominent treatment-related tracer accumulation in the bone marrow and salivary glands [13].

Weak tracer accumulation in the glandular tissue and bone marrow, detected on the baseline images, is consistent with spontaneous apoptosis as part of the homeostatic regulation of cell number and differentiation [14–16]. Intense early post-treatment salivary gland annexin V uptake, confined to the radiation field, is most likely due to radiation-induced apoptosis in the serous gland cells as demonstrated by Stephens et al. [17]. This phenomenon was also extensively described during the early phase of gland reaction in a preclinical study performed by the group of Paardekooper [18] and in the review by Guchelaar et al. [19]. Zheng et al. have demonstrated that quantitative analysis of the changes in tracer uptake by the salivary glands may offer prognostic information regarding salivary gland damage and function, and could eventually be useful as a biomarker of a patient's susceptibility to radiation-induced salivary dysfunction [20]. Similarly, chemotherapy- and field-related radiotherapy-induced bone marrow tracer accumulation reflects intramedullary apoptosis and correlates well with the results of preclinical studies performed by the group of Blankenberg [21]. This group demonstrated the feasibility of non-invasive monitoring and quantification of therapy-induced intramedullary apoptosis by annexin V imaging.

Interestingly, evaluation of patients with a previous history of radiation shows weak annexin V uptake in the irradiated bone marrow, which does not change early after the start of radiotherapy and/or chemotherapy. Perhaps this can be explained by different radiosensitivities and regrowth potential of the stromal and haemopoietic components. Several studies have shown that stromal tissue regrows rapidly, while haemopoietic tissue does not regenerate and is mainly replaced by adipocytes [22, 23]. This suggests that a post-treatment increase in the bone marrow tracer uptake is mainly caused by apoptosis in the haematopoietic tissue. Stromal cell apoptosis, described by Anton [24], may contribute to the tracer uptake but probably does not play a significant role. Based on these observations, early post-treatment evaluation of bone marrow uptake of annexin V could allow monitoring of the myelosuppressive effect of the treatment regimen on a patient-by-patient basis.

In conclusion, co-registration of ^{99m}Tc-Hynic-rh-annexin V SPECT and CT allows precise mapping of the ^{99m}Tc-Hynic-rh-annexin V distribution in tumour and normal tissues for detailed evaluation of apoptosis before and early after the start of chemotherapy and/or radiotherapy. The relationship between tracer distribution in the bone marrow and salivary glands and treatment regimen found in this study may contribute to the evaluation of dose–effect relations in various treatment schedules. TAS may therefore be used as a non-invasive method to evaluate antitumour effects, to predict the severity of the normal tissue toxicity and to assess the effectiveness of protective drugs.

References

1. Blankenberg FG, Katsikis PD, Tait JF, Davis RE, Naumovski L, Ohtsuki K, et al. In vivo detection and imaging of phosphatidylserine expression during programmed cell death. Proc Natl Acad Sci U S A 1998;95:6349–6354
2. Belhocine T, Steinmetz N, Li C, Green A, Blankenberg FG. The imaging of apoptosis with the radiolabeled annexin V: optimal timing for clinical feasibility. Technol Cancer Res Treat 2004;3:23–32
3. Belhocine T, Steinmetz N, Green A, Rigo P. In vivo imaging of chemotherapy-induced apoptosis in human cancers. Ann N Y Acad Sci 2003;1010:525–529
4. Belhocine T, Steinmetz N, Hustinx R, Bartsch P, Jerusalem G, Seidel L, et al. Increased uptake of the apoptosis-imaging agent (99m)Tc recombinant human Annexin V in human tumors after one course of chemotherapy as a predictor of tumor response and patient prognosis. Clin Cancer Res 2002;8:2766–2774
5. Kartachova M, Haas RL, Valdes Olmos RA, Hoebers FJ, Van Zandwijk N, Verheij M. In vivo imaging of apoptosis by (99m) Tc-Annexin V scintigraphy: visual analysis in relation to treatment response. Radiother Oncol 2004;72:333–339

6. Kuge Y, Sato M, Zhao S, Takei T, Nakada K, Seki KI, et al. Feasibility of ^{99m}Tc-annexin V for repetitive detection of apoptotic tumor response to chemotherapy: an experimental study using a rat tumor model. J Nucl Med 2004;45:309–312
7. Kramer EL, Noz ME. CT-SPECT fusion for analysis of radiolabeled antibodies: applications in gastrointestinal and lung carcinoma. Int J Rad Appl Instrum B 1991;18:27–42
8. Loats H. CT and SPECT image registration and fusion for spatial localization of metastatic processes using radiolabeled monoclonals. J Nucl Med 1993;34:562–566
9. Schillaci O, Simonetti G. Fusion imaging in nuclear medicine —applications of dual-modality systems in oncology. Cancer Biother Radiopharm 2004;19:1–10
10. Kemerink GJ, Liem IH, Hofstra L, Boersma HH, Buijs WC, Reutelingsperger CP, et al. Patient dosimetry of intravenously administered ^{99m}Tc-annexin V. J Nucl Med 2001;42:382–387
11. Kemerink GJ, Liu X, Kieffer D, Ceyssens S, Mortelmans L, Verbruggen AM, et al. Safety, biodistribution, and dosimetry of ^{99m}Tc-HYNIC-annexin V, a novel human recombinant annexin V for human application. J Nucl Med 2003;44:947–952
12. Haas RL, de Jong D, Valdes Olmos RA, Hoefnagel CA, van den Heuvel I, Zerp SF, et al. In vivo imaging of radiation-induced apoptosis in follicular lymphoma patients. Int J Radiat Oncol Biol Phys 2004;59:782–787
13. Vermeersch H, Loose D, Lahorte C, Mervillie K, Dierckx R, Steinmetz N, et al. ^{99m}Tc-HYNIC annexin-V imaging of primary head and neck carcinoma. Nucl Med Commun 2004;25:259–263
14. DeLong MJ. Apoptosis: a modulator of cellular homeostasis and disease states. Ann N Y Acad Sci 1998;842:82–90
15. Domen J, Cheshier SH, Weissman IL. The role of apoptosis in the regulation of hematopoietic stem cells: overexpression of Bcl-2 increases both their number and repopulation potential. J Exp Med 2000;191:253–264
16. Ekert PG, Vaux DL. Apoptosis, haemopoiesis and leukaemogenesis. Baillieres Clin Haematol 1997;10:561–576
17. Stephens LC, Schultheiss TE, Price RE, Ang KK, Peters LJ. Radiation apoptosis of serous acinar cells of salivary and lacrimal glands. Cancer 1991;67:1539–1543
18. Paardekooper GM, Cammelli S, Zeilstra LJ, Coppes RP, Konings AW. Radiation-induced apoptosis in relation to acute impairment of rat salivary gland function. Int J Radiat Biol 1998;73:641–648
19. Guchelaar HJ, Vermes A, Meerwaldt JH. Radiation-induced xerostomia: pathophysiology, clinical course and supportive treatment. Support Care Cancer 1997;5:281–288
20. Zheng R, Dahlstrom KR, Wei Q, Sturgis EM. Gamma radiation-induced apoptosis, G2 delay, and the risk of salivary and thyroid carcinomas—a preliminary report. Head Neck 2004;26:612–618
21. Blankenberg FG, Naumovski L, Tait JF, Post AM, Strauss HW. Imaging cyclophosphamide-induced intramedullary apoptosis in rats using ^{99m}Tc-radiolabeled annexin V. J Nucl Med 2001;42:309–316
22. Argiris A, Maris T, Papavasiliou G, Gouliamos A, Papavasiliou C. Radiotherapy effects on vertebral bone marrow: easily recognizable changes in T2 relaxation times. Magn Reson Imaging 1996;14:633–638
23. Meyer MA, Nathan CA. Reduced F-18 fluorodeoxyglucose uptake within marrow after external beam radiation. Clin Nucl Med 2000;25:279–280
24. Anton E. Ultrastructural changes of stromal cells of bone marrow and liver after cyclophosphamide treatment in mice. Tissue Cell 1997;29:1–9